Mathematical Tools for Instrumentation & Signal Processing in Astronomy
D. Mary, R. Flamary, C. Theys and C. Aime (eds)
EAS Publications Series, ***78-79*** *(2016) 275–285*

PSF HOMOGENIZATION FOR MULTI-BAND PHOTOMETRY FROM SPACE ON EXTENDED OBJECTS

A. Boucaud[1,2], H. Dole[1], A. Abergel[1], H. Ayasso[3] and F. Orieux[1,4]

Abstract. We present a fast and robust tool to create PSF matching kernels for multi-band photometric studies. Such kernels are useful for convolving images down to the same PSF prior to computing flux measurements like aperture photometry or spectral fitting. Unlike similar existing methods, we use a Wiener filter to take into account the real shape of the effective PSF, usually very complex for space telescopes. We apply this scheme to Euclid simulated PSF images to demonstrate the efficiency of the algorithm. This tool is publicly available at `http://www.github.io/aboucaud/pypher`.

1 Introduction

Although the 21st century has witnessed the emergence of hyper-spectral astronomy data (*i.e.* spatially resolved spectra of large regions of the sky) with projects like BOSS (Schlegel *et al.* 2007) or the more recent MUSE (Bacon *et al.* 2010), the vast majority of the sky is still only covered by imagers like *e.g.* SDSS (Kent 1994), CFHTLS (Cabanac *et al.* 2007), DES (Dark Energy Survey Collaboration *et al.* 2005) in the optical; IRAS (Neugebauer *et al.* 1984), 2MASS (Skrutskie *et al.* 2006), WISE (Wright *et al.* 2010) in the infrared and NVSS (Condon *et al.* 2002), Fermi (Atwood *et al.* 2009) or Planck (Planck Collaboration *et al.* 2015) at other wavelengths. The angular resolution of such instruments – including the optical path inside the telescope and the instruments, as well as the detector response, the sampling strategy and the potential atmospheric transmitance – is

[1] Institut d'Astrophysique Spatiale, CNRS, UMR 8617, Université Paris-Sud, Université Paris-Saclay, IAS, Bât. 121, 91405 Orsay, France; e-mail: `alexandre.boucaud@ias.u-psud.fr`

[2] Sorbonne Universités, UPMC Université Paris 6 et CNRS, UMR 7095, Institut d'Astrophysique de Paris, 98 bis Bd. Arago, 75014 Paris, France

[3] GIPSA-LAB, 11 rue des Mathématiques, 38402 Saint-Martin-d'Hères, France

[4] Laboratoire des Signaux et Systèmes, Université Paris-Sud, CNRS, Centrale Supélec, Université Paris-Saclay, 91192 Gif-sur-Yvette, France

DOI: 10.1051/eas/1678013

characterised by the point spread function (PSF). The PSF, also known as *beam*, depends on the wavelength of the observation through the laws of diffraction.

When multi-band images are the only available data, we can try to recover some spectral information of astronomical objects. This can be done with the use of either photometric bands on a single detector (*e.g.* filters); various detectors within an instrument (*e.g.* CCDs, bolometers), providing a sensitivity to a broader range of wavelengths; multiple instruments pointing on common fields; or a combination of these options. In order to compute the colors of the objects (*i.e.* ratio of observed flux in two bands) on multi-band images, both aperture photometry and model fitting photometry can be used. Both techniques require an accurate knowledge of the point spread function on each image to be able to measure object fluxes in each band, to account for the different angular resolution and sampling of the various observations. One method that has been fairly used over the last decades is called PSF homogenization. It consists of using the PSF model of both observations to compute a matching kernel between the two images. The kernel is then convolved with the highest angular resolution image to match the resolution of the second image. Once at the same angular resolution, the flux measurement on both images is coherent and the colors can thus be determined.

At the era of upcoming observatories such as JWST (Gardner *et al.* 2006) or all-sky survey photometric missions such as LSST (LSST Science Collaboration *et al.* 2009) or Euclid (Laureijs *et al.* 2010), crucial information like the photometric redshift of the objects will only be obtained using additional photometric information from other existing surveys like DES (Dark Energy Survey Collaboration *et al.* 2005), Pan-STARRS (Kaiser *et al.* 2010) or KiDS (de Jong *et al.* 2013) and observatories such as XMM (Mason *et al.* 2001), Herschel (Pilbratt *et al.* 2010) or Spitzer (Werner *et al.* 2004). To allow for these multi-band studies to be performed, it is key to have a robust matching kernel generation algorithm.

Current methods developed in astronomy fall into two main categories, on the one hand those depending of an analytic description of the PSF to create analytical formulæ for the kernels, and on the other hand the methods we call *pixel-based*, that are focused on using the observed or simulated PSF to date, also referred to as the *effective* PSF.

Among the analytic descriptions of the PSF, the most widely spread is the two- dimensional Gaussian approximation, that has the advantage of providing an analytical formula for the matching kernel. It has been used thoughout the years as a reliable method for homogenizing images, especially for ground-based data blurred by the atmosphere. In the past decade, a refined PSF description known as polar shapelets was invented by Massey and Refregier (2005) and gained traction, especially in the weak lensing community. This formalism was used *e.g.* by Kuijken (2008) to propose a method called re-Gaussianization, whose purpose is to capture a decomposition of the PSF across an image and create a varying kernel to transform that PSF into a predefined gaussian one. This process has been used by several large surveys as KiDS and the CFHTLens (Hildebrandt *et al.* 2012).

On the pixel-based side, an approach to PSF homogenization was taken in the late nineties by Alard & Lupton (1998) in the context of transient object study

from ground-based telescopes. They presented a method for computing convolution kernels to correct for the impact of varying atmospheric conditions on the PSF and improve the subtraction of images of the same patches of sky. Following this idea, but concentrating on homogenizing multi-band data, Gordon *et al.* (2008) computed kernels for all the combinations between bands and instruments of Spitzer & Herschel infrared satellites, using a mix of simulated and observed PSFs. More recently, in a similar vein of Gordon *et al.* (2008), Aniano *et al.* (2011) proposed a method to generate convolution kernels for a wider range of cameras/telescopes, including satellites and ground-based ones, with the prescription that PSFs are close enough of having rotational symmetry that they can be circularized and defined by their radial profile. Such approximations can no longer be considered when attacking precision photometry on multi-wavelength data, where the whole PSF shape and details must be taken into account.

In this paper we propose a method to compute a matching kernel given stationnary effective PSFs, based on a regularized Wiener filter algorithm. Since there is no model accurate enough to fully describe and characterize the observed complexity of actual instrumental PSFs, we denote here, by *effective*, the best PSF approximation that is available for a given instrument. Such PSF can be obtained from simulations (ray tracing using the telescope optical design), with calibrated data (*e.g.* pointings to dim/bright objects in order to respectively characterize the core/tails of the PSF), or from a more traditional set of bright unsaturated stars on the exposures.

In the following, we describe the method and algorithm to produce robust and accurate homogenization kernels, and show an application to Euclid simulated data. A more detailed study of the impact of using such method on *Herschel* data compared to the previous ones (*e.g.* Aniano *et al.* 2011) shall be exposed in Boucaud *et al.* (2016, *in prep.*).

2 Methods

2.1 Problem definition

Let's first consider an astrophysical observed image $\boldsymbol{y}$, modeled as a linear invariant system:

$$\boldsymbol{y} = \boldsymbol{H}\boldsymbol{x} + \boldsymbol{n}, \tag{2.1}$$

where $\boldsymbol{H}$ is the linear operator modeling the convolution between the PSF and the unknown sky $\boldsymbol{x}$, and n is the image noise. Considering now two instruments/bands a and b and their respective PSF model $\boldsymbol{H}_a$ and $\boldsymbol{H}_b$, an image $\boldsymbol{y}_a$ acquired by a can be expressed as

$$\boldsymbol{y}_a = \boldsymbol{H}_a\boldsymbol{x} + \boldsymbol{n}_a. \tag{2.2}$$

The purpose of homogenization is to obtain an image $\boldsymbol{y}_{a,b}$ which displays the information of image $\boldsymbol{y}_a$ as it would be observed at the angular resolution of b. To this end, this paper presents a linear algorithm that computes a matching kernel

$\boldsymbol{k}_a^b$ that produces a PSF-matched image $\boldsymbol{y}_{a,b}$ through a convolution with $\boldsymbol{y}_a$

$$\begin{aligned} \boldsymbol{y}_{a,b} &= \boldsymbol{k}_a^b * \boldsymbol{y}_a, && (2.3)\\ &= \boldsymbol{H}_a^b \boldsymbol{y}_a, && (2.4)\\ &\simeq \boldsymbol{H}_b \boldsymbol{x}, && (2.5) \end{aligned}$$

where $*$ stands for the discrete convolution and $\boldsymbol{H}_a^b$ is the convolution operator that matches the PSF model of a to the model of b.

Compared to previous work, the kernels presented in this work are much more accurate than the one currently considered as standard like those produced by Aniano *et al.* (2011).

2.2 Kernel generation

To produce the kernels, one first needs to get an estimate $\hat{\boldsymbol{x}}$ of the unknown sky, and then convolve that estimate with the PSF model of the target instrument/band. While the second step is straightforward, the estimation of the unknown sky requires a system inversion, also known as deconvolution, which must be treated with specific care.

For linear systems such as (2.1), one can seek an estimate of $\boldsymbol{x}$, denoted $\hat{\boldsymbol{x}}$, that minimizes the least squares criterion $J(\boldsymbol{x})$

$$\begin{aligned} \hat{\boldsymbol{x}} &= \arg\min_{\boldsymbol{x}} J(\boldsymbol{x}), && (2.6)\\ &= \arg\min_{\boldsymbol{x}} \|\boldsymbol{y} - \boldsymbol{H}\boldsymbol{x}\|^2. && (2.7) \end{aligned}$$

However, the presence of the convolution makes the system ill-posed for the inversion and there is no stable solution to Equation (2.7). The only way to stabilize the solution is to add information. For the considered system, we use a technique called *regularization*. Since we want to impose a linear filtering, and thus choose to add an ℓ_2 penalization to the least square criterion. In addition, as we expect the noise in the image to be subdominant compared to the PSF level, we penalize the high-frequencies. This corresponds to adding a relative degree of smoothness between values of neighboring pixels. The new criterion is

$$J(\boldsymbol{x}) = \|\boldsymbol{y} - \boldsymbol{H}\boldsymbol{x}\|^2 + \mu \|\boldsymbol{D}\boldsymbol{x}\|^2, \quad (2.8)$$

where $\boldsymbol{D}$ is the second order differential operator (high-pass filter) and μ the regularization parameter. The latter tunes the balance between the data fidelity and the penalization.

Under the circular boundary condition hypothesis and denoting the Fourier transform by $\boldsymbol{F}$, we can write

$$\begin{aligned} \boldsymbol{H} &= \boldsymbol{F}^\dagger \Lambda_{\boldsymbol{H}} \boldsymbol{F}, && (2.9)\\ \boldsymbol{D} &= \boldsymbol{F}^\dagger \Lambda_{\boldsymbol{D}} \boldsymbol{F}, && (2.10) \end{aligned}$$

where $\Lambda_{\boldsymbol{H}}$ and $\Lambda_{\boldsymbol{D}}$ are diagonal operators. With that in mind, the cancellation of the first gradient of the criterion (2.8) leads to the classical solution

$$\hat{\boldsymbol{x}} = \boldsymbol{F}^{\dagger}\Lambda_{\boldsymbol{W}}\boldsymbol{F}\boldsymbol{y} \quad \text{with} \quad \Lambda_{\boldsymbol{W}} = \frac{\Lambda_{\boldsymbol{H}}^{\dagger}}{|\Lambda_{\boldsymbol{H}}|^2 + \mu\,|\Lambda_{\boldsymbol{D}}|^2}, \tag{2.11}$$

where $\Lambda_{\boldsymbol{W}}$ is a Wiener filter.

Once the unknown sky has been estimated, the final matching is achieved by applying the convolution operator of the target instrument, *i.e.* $\boldsymbol{H}_b$ to the estimated sky, following the example of Equation (2.5). Under the same assumption as Equation (2.9), this convolution can be performed in Fourier space, leading to the operator $\boldsymbol{H}_a^b$ of Equation (2.4) being computed with the expression

$$\boldsymbol{H}_a^b = \boldsymbol{F}^{\dagger}\Lambda_{\boldsymbol{H}_a^b}\boldsymbol{F} \quad \text{with} \quad \Lambda_{\boldsymbol{H}_a^b} = \frac{\Lambda_{\boldsymbol{H}_b}\Lambda_{\boldsymbol{H}_a}^{\dagger}}{|\Lambda_{\boldsymbol{H}_a}|^2 + \mu\,|\Lambda_{\boldsymbol{D}}|^2}. \tag{2.12}$$

The homogenization kernel $\boldsymbol{k}_a^b$ from Equation (2.3), whose generation is the purpose of this paper, is obtained using the latter formula (2.12) and only requires the source and target PSF models, respectively, $\boldsymbol{H}_a$ and $\boldsymbol{H}_b$ and a non-zero regularization parameter μ. Specific directives on the use of μ will be discussed in Section 4.1.

2.3 *Pypher*

A Python code that produces the stationary PSF homogenization kernels $\boldsymbol{k}_a^b$ has been made publicly available and can be retrieved at `http://www.github.io/aboucaud/pypher`.

Once installed, this program can be used through a command-line interface taking as input the PSF images – source and target – as fits files, and specifying the output filename for the kernel. The simplest command in a terminal to produce a kernel is

```
$ pypher psf_a.fits psf_b.fits kernel_a_to_b.fits
```

Then there are some options that can be tuned according to the PSF images and the science images to homogenize:

- the regularization parameter μ of the Wiener filter (see Eq. (2.11)) that penalizes the high-frequencies, and should be set according to the image that will be homogenized,
- the input PSFs position angle with respect to their image to accurately take into account the shape of both PSF in the homogenization process.

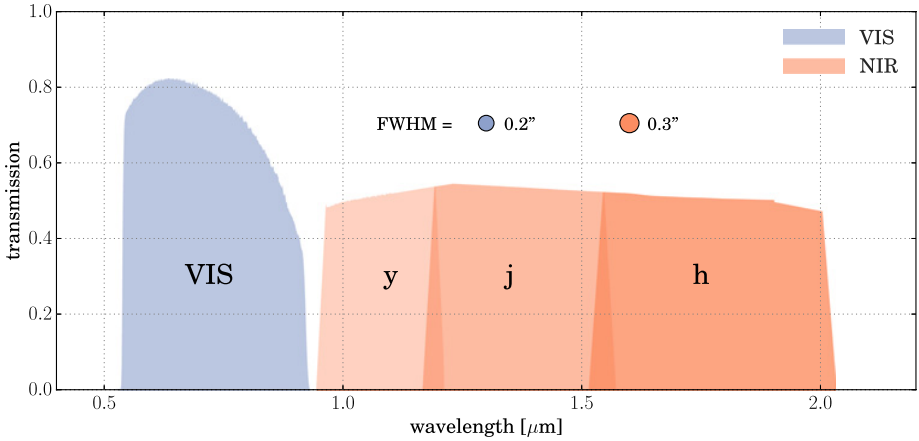

Fig. 1. Euclid preliminary photometric bandpasses (2015), *i.e.* transmission *vs.* wavelength, with their associated angular resolution expressed in terms of the FWHM.

3 Application to Euclid simulations

3.1 Euclid context

Euclid (Laureijs *et al.* 2011) is an M-class mission of the European Space Agency (ESA), due to launch in 2021. It is a cosmology experiment designed to measure the large scale structure of the Universe with exquisite accuracy over 15 000 sq.deg. There are two main science goals: one is to carry out a redshift survey of distant galaxies; the other is to make a galaxy weak lensing survey.

The Euclid satellite has two focal place imaging instruments: VIS (Cropper *et al.* 2014) having one broad band optical filter, and NISP (Prieto *et al.* 2012) having three near-infrared filters called y, j and h plus spectroscopic capabilities. The preliminary throughput for the four photometric bands is shown on Figure 1. The purpose of this study is to create convolution kernels that can be applied to images from one band to emulate the resolution of another band with lower angular resolution.

On Figure 2 preliminary simulations of the broadband PSF of each Euclid photometric channel are shown. They provide an insight of the complexity of the optical system and the related difficulty of properly computing kernels for such systems. One can note the non negligible power stored in the wings of the PSFs, that extend up to 40 arcseconds from the center ($\sim 200 \times$ FWHM).

The comparison of this spatial extent with the size of the FHWM, *i.e.* between 0.1 and 0.3 arcseconds, underlines the failure of the current models. On the one hand, the power stored in a gaussian profile drops so quickly that it cannot have the right FWHM and an accurate spatial distribution of the power. On the other hand, a simple radial profile comming from the circularization procedure wipes

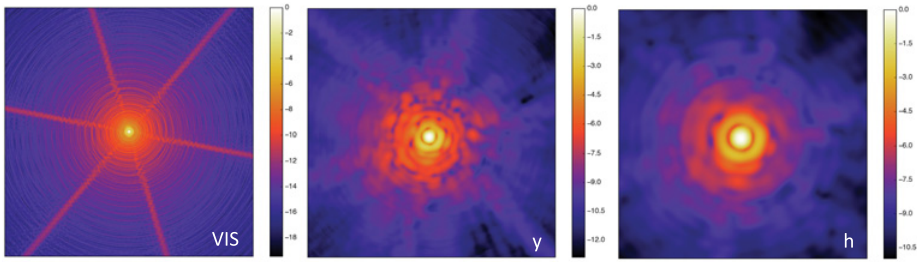

Fig. 2. Early simulations of the Euclid photometric band PSFs (2014), respectively from *left* to *right*, the optical band VIS, the y-band and the h-band in NIR. The image colors are logarithmically stretched and their angular size is 40×40 arcseconds. These preliminary broadband PSFs have been obtained using ray tracing in an optical model of the telescope and instruments.

out the shape of the wings by radially averaging the power, which also tends to dilute their effect, especially when tackling separate astrophysical sources.

3.2 Matching test between VIS and h-band

In the following, we denote a Euclid PSF image by $\boldsymbol{\phi}$ and a kernel image by the two-dimensional matrix $\boldsymbol{k}$.

In order to test the algorithm, we performed a procedure that can be summarized in three steps:

1. Compute the kernel $\boldsymbol{k}_a^b$ between $\boldsymbol{\phi}_a$ and $\boldsymbol{\phi}_b$
2. Convolve $\boldsymbol{\phi}_a$ with the kernel to produce $\boldsymbol{\phi}_{a,b}$
3. Compare the resulting matched PSF $\boldsymbol{\phi}_{a,b}$ to the original PSF $\boldsymbol{\phi}_b$.

The final comparison is made through a computation of the residus,

$$\boldsymbol{R}_{a,b} = \frac{\boldsymbol{\phi}_b - \boldsymbol{\phi}_{a,b}}{\boldsymbol{\phi}_{b,\max}} = \frac{\boldsymbol{\phi}_b - \boldsymbol{\phi}_a * \boldsymbol{k}_a^b}{\boldsymbol{\phi}_{b,\max}}. \tag{3.13}$$

We applied this procedure to the Euclid VIS and h-band PSFs and the resulting kernel and residus plots are shown on Figure 3. The log-stretched image of the kernel on the left side of Figure 3 looks very much like the h-band PSF, as suspected, but shows additional low amplitude features towards the borders of the image that most probably correspond to the signature of VIS PSF wings.

The image of the residus on the right of Figure 3 has a very low amplitude $\boldsymbol{R}_{\mathrm{VIS},h} < 10^{-6}$ and shows a different pattern than that of the kernel or the respective PSFs in terms of the PSFs outskirts. However, we see that most of the highest residus are concentrated in the PSF center. To better understand this

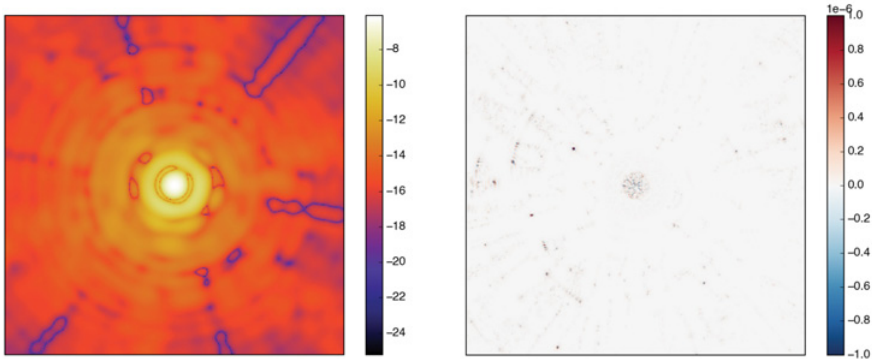

Fig. 3. Kernel generation and performance assessment with Euclid simulated data. The *left* image shows the kernel $\boldsymbol{k}^h_{\mathrm{VIS}}$ produced with $\mu = 10^{-6}$ to match the Euclid VIS PSF to the Euclid h-band one, both seen on Figure 2. The color display is logarithmically stretched to enhance the details. The *right* image corresponds to the residus $\boldsymbol{R}_{\mathrm{VIS},h}$ of the relative difference between the h-band PSF and the VIS PSF matched to the h-band using the kernel on the *left*.

phenomenon, we computed the power spectral density (PSD) of each of the involved images, resulting in Figure 4.

The PSD of an image is a visualization of the amount of power for a given frequency, that corresponds to a characteristic size in the image. The quite constant power spectral density of the residuals (pink line on Fig. 4) shows that the homogenization process behaved well and that no particular frequency was amplified, especially the high-frequency part of the spectrum that corresponds to image noise. The limitation of the matching procedure is seen through the difference between the PSD of the original PSF in orange and the matched PSF in blue. Fortunately, that difference appears after the cutting frequency of the image, at a level only affected with noise. That power difference at high frequencies can be interpreted as the intrinsic denoising feature of the Wiener filtering, whose amplitude is proportional to the regularisation parameter μ that appears in Equations (2.8), (2.11) and (2.12).

The matched image being denoised by the Wiener filter, the subtraction step of the residus computation only keeps high frequency wiggles in the image. Our explanation for the central part localization of the residus is that the normalisation to the maximum value of the original image in the computation favors the peek values as opposed to the outskirts of the image.

4 Algorithm performance

4.1 The μ regularization parameter

The regularization parameter, μ, is the only tunable parameter in this algorithm. Orieux *et al.* (2010) have shown that an optimal value exists for μ, which

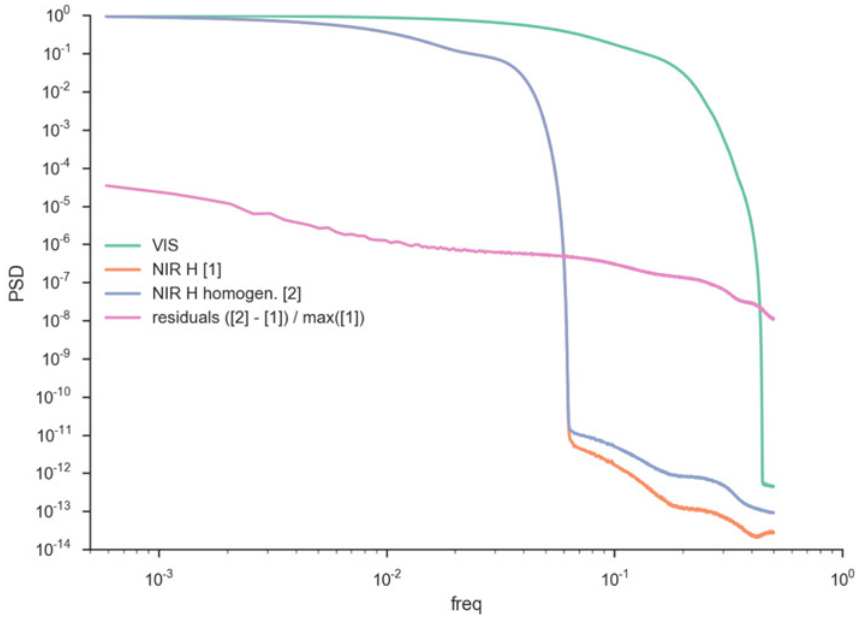

Fig. 4. Power spectral density (PSD) of the VIS, h-band, VIS matched to h-band PSFs, and the residuals (*cf.* right image on Fig. 3). The PSD describes the intensity as a function of the frequency in the image.

corresponds to the signal-to-noise ratio of the image to be matched. That optimal value can be determined though an iterative procedure, which is not yet implemented in `pypher`. Instead, the code currently prompts the user for a specific value for μ or uses the default value $\mu = 10^{-4}$.

4.2 Computing efficiency

Kernel computation is very fast. The `pypher` program takes less than a second on a single CPU to compute a kernel from two 512×512 PSF images. Therefore, for most applications, kernels do not need be to computed and stored in advance but can be generated when needed in a pipeline.

Concerning the matching process – the convolution of the image with the kernel – the computation time for a given image depends on the size of the kernel. Since our method uses the effective PSF without any prior modeling or transformation, the kernel size (in pixels) is the same as the biggest input PSF, in array-size. For this reason, a real-space convolution with big images might be slow and the kernel must sometimes be trimmed down to a smaller size, while making sure most of the flux is conserved. Or the convolution must be performed in Fourier space (small overhead but generally much faster).

5 Conclusion

In this work, we have developed and implemented a robust and very efficient algorithm for the generation of matching kernels between two PSFs. Compared to similar homogenization methods, this procedure does not assume any particular analytical shape or symmetrical properties for the input PSFs, but uses the full available information on the PSF. It is aimed at recovering as much power as possible, even concentrated in pencil-shaped wings far from the peak. This algorithm thus provides an unprecedented accuracy for homogenizing astronomical images for multi-wavelength photometric studies, especially when dealing with the complex features of effective PSFs inherent to space telescopes.

The tests on simulated Euclid images have demonstrated a great success with very low residuals on the reconstruction of the target PSF. Further tests and analysis on Herschel data, using this algorithm, will be presented in Boucaud *et al.* (2016, *in prep.*). Finally, the code to produce these kernels can be download at `http://www.github.io/aboucaud/pypher`.

References

Alard, C., & Lupton R.H., 1998, ApJ, 503, 325

Aniano, G., Draine, B., Gordon, K., & Sandstrom, K., 2011, PASP, 123, 1218

Atwood, W., Abdo, A.A., Ackermann, M., *et al.*, 2009, ApJ, 697, 1071

Bacon, R., Accardo, M., Adjali, L., *et al.*, 2010, The Muse Second-Generation vlt Instrument, SPIE Astron. Teles.+ Instrum., Inter. Soc. Opt. Phot., p. 773508

Boucaud, A., Bocchio, M., Abergel, A., *et al.*, 2016, A&A, in preparation

Cabanac, R., Alard, C., Dantel-Fort, M., *et al.*, 2007, A&A, 461, 813

Condon, J., Cotton, W., Greisen, E., *et al.*, 2002, Vizier online data catalog: 1.4 ghz nrao vla sky survey (nvss)(condon+ 1998). VizieR Online Data Catalog, 8065:0

Cropper, M., Pottinger, S., Niemi, S.-M., *et al.*, 2014, VIS: the visible imager for Euclid, SPIE Astron. Teles.+ Instru., Intern. Soc. Opt. and Phot., p. 91430J

Dark Energy Survey Collaboration *et al.*, 2005, The Dark Energy Survey, `arXiv preprint` [`astro-ph/0510346`]

de Jong, J.T., Kleijn, G.A.V., Kuijken, K.H., *et al.*, 2013, Exper. Astron., 35, 25

Gardner, J.P., Mather, J.C., Clampin, M., *et al.*, 2006, Space Sci. Rev., 123, 485

Gordon, K.D., Engelbracht, C.W., Rieke, G.H., *et al.*, 2008, ApJ, 682, 336

Hildebrandt, H., Erben, T., Kuijken, K., *et al.*, 2012, MNRAS, 421, 2355

Kaiser, N., Burgett, W., Chambers, K., *et al.*, 2010, The Pan-STARRS wide-field optical/NIR imaging survey, SPIE Astron. Teles.+ Instru., Intern. Soc. Opt. Phot., p. 77330E

Kent, S.M., 1994, Sloan Digital Sky Survey, Science with Astronomical Near-Infrared Sky Surveys (Springer), p. 27

Kuijken, K., 2008, A&A, 482, 1053

Laureijs, R., Amiaux, J., Arduini, S., *et al.*, 2011, Euclid definition study report, `arXiv preprint` [`arXiv:1110.3193`]

Laureijs, R.J., Duvet, L., Sanz, I.E., *et al.*, 2010, SPIE Astron. Teles.+ Instru., Intern. Soc. Opt. Phot., p. 77311H

LSST Science Collaboration, *et al.*, 2009, LSST science book, version 2.0, `arXiv`, 912

Mason, K., Breeveld, A., Much, R., *et al.*, 2001, A&A, 365, L36

Massey, R., Refregier, A., 2005, MNRAS, 363, 197

Neugebauer, G., Habing, H., Van Duinen, R., *et al.*, 1984, ApJ, 278, L1

Orieux, F., Giovannelli, J.-F., & Rodet, T., 2010, JOSA A, 27, 1593

Pilbratt, G., Riedinger, J., Passvogel, T., *et al.*, 2010, A&A, 518, L1

Planck Collaboration, Adam, R., Ade, P., Aghanim, N., *et al.*, 2015, Planck 2015 results. i. overview of products and scientific results, `arXiv preprint` [`arXiv:1502.01582`]

Prieto, E., Amiaux, J., Auguères, J.-L., *et al.*, 2012, Euclid near-infrared spectrophotometer instrument concept at the end of the phase A study, SPIE Astron. Teles.+ Instru., Intern. Soc. Opt. Phot., p. 84420W

Schlegel, D.J., Blanton, M., Eisenstein, D., *et al.*, 2007, BAAS, 39, 966

Skrutskie, M., Cutri, R., Stiening, R., *et al.*, 2006, AJ, 131, 1163

Werner, M., Roellig, T., Low, F., *et al.*, 2004, ApJS, 154, 1

Wright, E.L., Eisenhardt, P.R., Mainzer, A.K., *et al.*, 2010, AJ, 140, 1868